Biochimica et Biophysica Acta, 974 (1989) 88–103
Elsevier

BBA 42970

Isotropic and linear dichroic triplet-minus-singlet absorbance difference spectra of two carotenoid-containing bacterial photosynthetic reaction centers in the temperature range 10–288 K. An analysis of bacteriochlorophyll-carotenoid triplet transfer

E.J. Lous * and A.J. Hoff

Department of Biophysics, Huygens Laboratory of the University of Leiden, Leiden (The Netherlands)

(Received 5 January 1989)

Key words: Triplet transfer; Carotenoid; Photosynthetic reaction center; (*Rb. sphaeroides* 2.4.1); (*R. rubrum* S1)

Isotropic and linear dichroic triplet–minus–singlet (T − S) spectra of reaction centers of *Rhodobacter sphaeroides* 2.4.1 and *Rhodospirillum rubrum* S1 have been measured with magneto-optical difference spectroscopy (MODS) in the wavelength range 350–950 nm as a function of the temperature (10–288 K). The (T − S) spectra allowed the determination of the carotenoid triplet yield and the probability of triplet transfer between the primary donor bacteriochlorophyll *a* (BChl *a*) dimer, D, and the carotenoid as a function of the temperature. The $^3D \rightarrow {}^3C$ transfer can be described with an equilibrium model, without introducing additional triplet states. The $^3D \rightarrow {}^3C$ transfer has an activation enthalpy of 0.020 eV, while the activation enthalpy of the backward transfer is 0.15 eV for *Rb. sphaeroides* 2.4.1 and 0.08 eV for *R. rubrum* S1 and apparently depends on the type of carotenoid present in the reaction center (spheroidene in *Rb. sphaeroides* 2.4.1, spirilloxanthin in *R. rubrum* S1). The energies of the spheroidene and the spirilloxanthin triplet states in the reaction center are 0.81 and 0.88 eV, respectively. The protection against free oxygen by the carotenoid at physiological temperatures is therefore better in *Rb. sphaeroides* 2.4.1 than in *R. rubrum* S1. The mechanism of triplet transfer between dimer and carotenoid is discussed. It is suggested that one possible mechanism may involve a change in triplet localization of ^3D, populating the higher-energy triplet exciton state of ^3D. Evidence has been found that ^3C shares its triplet exciton with an accessory BChl *a* and that with increasing temperature the triplet state on ^3D becomes more delocalized. The temperature-dependence of the energy and bandwidth of the low-exciton band of D, D(−), is interpreted to be mainly a consequence of thermal broadening and expansion of the BChl *a* dimer. The effect of a magnetic field on the yield of ^3D and ^3C depends on the temperature. This temperature-dependence is explained by two different magnetic-field effect mechanisms with different anisotropic properties, the radical pair mechanism at higher temperatures and the effect of magnetic field-induced mixing of the triplet sublevels at temperatures below about 50 K.

Introduction

RC structure

Reaction centers (RC) of purple photosynthetic bacteria contain four bacteriochlorophylls (BChl *a*), two bacteriopheophytins (BPh) and two quinones (Q). Two of the bacteriochlorophylls form a dimer (D), which functions as the primary electron donor, one BChl (B_A), one BPh (ϕ_A) and Q_A are arranged in an electron acceptor chain (the active or A chain), the

* Present address: Department of Physics, University of California, San Diego, La Jolla, CA 92093, U.S.A.

Abbreviations: ADMR, absorbance-detected magnetic resonance; BChl *a*, bacteriochlorophyll *a*; BPh *a*, bacteriopheophytin *a*; C, carotenoid; D, primary donor (BChl-dimer); D_A, primary donor BChl connnected to the L RC-protein subunit; D_B, primary donor BChl connected to the M RC-protein subunit; ISC, intersystem crossing; LD, linear dichroic; MIMS, magnetic field-induced mixing of triplet sublevels; MFE, magnetic field effect; MODS, magneto-optical difference spectroscopy; p.a.s., principal axes system of the zero-field dipole tensor, ***D***, of a triplet state; Q, quinone; Q_A, quinone connnected to the M RC-protein subunit; Q_B, quinone connnected to the L RC-protein subunit; RC, reaction center; RPM, radical pair mechanism; S, singlet; S–S, singlet–singlet; T, triplet; T–T, triplet–triplet; ϕ_A, BPh connected to the L RC-protein subunit; ϕ_B, BPh connected to the M RC-protein subunit.

Correspondence: A.J. Hoff, Huygens Laboratory, Rijksuniversiteit, Department of Biophysics, P.O. Box 9504, 2300 RA Leiden, The Netherlands.

other BChl (B_B) and BPh (ϕ_B) apparently are not involved in electron transport. The pigments subscripted by A are related to the B-subscripted ones by approximately C_2 symmetry [1–3]. After excitation of the primary donor D, directly or via excitation transfer, a radical pair state $^1[D^+\phi_A^-]$, is formed in 2.8 ps [4]. In native RC, stabilization of energy occurs by subsequent electron transport to Q_A, then to Q_B. Side-reactions such as triplet formation by 'indirect' ISC to ^3D via the $^3[D^+\phi_A^-]$ radical-pair state occur only with low probability.

Blocking light-induced electron transport along the active chain by prereduction or deletion of Q_A results in a much greater probability of formation of $^3[D^+\phi_A^-]$ and subsequently ^3D. The ^3D yield was found to increase from 0.10 at 300 K to almost unity at 10 K or lower [5].

The role of carotenoids

Wild-type RCs contain, in addition to the above pigments, a carotenoid molecule. Carotenoid is absent from some anaerobically living mutants, such as *Rb. sphaeroides* R-26. In addition to serving as a light-harvesting pigment, an important function of carotenoid is to protect against photochemical damage of the RC pigment-protein complex that is induced by the long-living, high-energy triplet state ^3D, by allowing triplet transfer from ^3D to the lower-energy ^3C state. The energy of ^3C is, in contrast to that of ^3D, too low to promote conversion of the $^3\Sigma$ dioxygen ground state into its highly reactive $^1\Delta_g$ singlet excited state (reviewed in Ref. 6).

The triplet-quenching efficiency of carotenoid in RCs will depend on the following: (i) The relative energies of the ^3C and ^3D states. The energy of the ^3C state is inversely proportional to the number of conjugated carbon bonds. (ii) The edge-to-edge distance between, and the relative orientation of, D and C, because triplet transfer is an exchange process that depends on orbital overlap of the electronic triplet wavefunctions. (iii) The extent of localization of the triplet state on the D dimer. Resonant Raman [7–9] and ultraviolet optical spectroscopy [9,10] studies indicate a 15-15′ mono-*cis* conformation of spheroidene in the RC of *Rb. sphaeroides* 2.4.1, neurosporene in *Rb. sphaeroides* G1C and spirilloxanthin in *Rhodosphirillum rubrum* S1. In addition, carotenoid in *Rb. sphaeroides* 2.4.1 may have out-of-plane twists at its outer end at the positions C-8–C-12 and/or C-8′–C-12′ [7]. No major structural change in the carotenoid polyene chain is induced by ^3C formation, either in its conformation or in the delocalized π-electron densities [11].

Carotenoids can be extracted and reconstituted, the latter also in carotenoidless mutant RC [12,13]. Polar functional groups on the carotenoid help it to gain access and to bind to polar residues in the protein and may promote triplet exchange with ^3D [13]. When carotenoid is present in the RC, borohydride-induced removal of the accessory B_B is more difficult [14]. This agrees with the observation of Deisenhofer et al. (personal communication and Ref. 15) and Allen et al. [16] that the carotenoid molecule is located close to B_B.

Magnetic field effects

The many open questions concerning position, function and electronic properties of carotenoids in photosynthetic RCs motivated us to utilize our recently developed MODS technique [17] to probe the triplet state of the carotenoid RC and its environment. With MODS, one is able to measure optical absorbance difference spectra of the RC with all the pigments in the ground state and of RC having a triplet state on one of its pigments (either D or C), so-called triplet-minus-singlet (T − S) absorbance difference spectra, in the temperature range 1.2–300 K [18,19]. With linear dichroic (LD)-MODS the anisotropy of these spectra with respect to a preferred axis is measured [19].

The MODS technique makes use of the dependence of the ^3D and ^3C concentrations on an external magnetic field. There are two fundamentally different mechanisms for this dependence: one acts on the probability of formation of the triplet states, the other on their decay rate. They are summarized below.

In RCs where electron transport to Q_A is blocked, ^3D is formed via the S–T transfer step $^1[D^+\phi_A^-] \rightarrow {}^3[D^+\phi_A^-]$ and subsequent radical recombination. This process is called the radical pair mechanism, RPM (reviewed in Ref. 20). According to the theory of the RPM, the $^1[D^+\phi_A^-]$ state mixes in zero-magnetic field with all the three $^3[D^+\phi_A^-]$ states. At high fields, however, only S–T_0 mixing is left so that the probability of ^3D formation is reduced by up to $\pm 45\%$ [21,22]. The curve of the yield of ^3D as a function of $|\boldsymbol{B}_0|$ is known as an MFE or MARY curve [23].

The RPM-induced MFE is expected to decrease with temperature, since k_S, the decay rate of $^1[D^+\phi_A^-]$, becomes very small at very low temperatures (below 77 K) [24]. (For $k_S = 0$, the RPM-induced MFE is zero). For non-spherically symmetric triplet states such as ^3C and ^3D, however, at temperatures below approx. 50 K, where spin-lattice relaxation (T_1) processes are slowed down, another MFE appears, which is caused by the mixing of the zero-field triplet eigenfunctions, that is induced by an applied stationary magnetic field (see for example, Ref. 25). Generally, the molecular decay rates k_i and the population probabilities p_i of each triplet sublevel in zero field are different. The magnetic field-induced mixing of the sublevels occasions a mixing of the k_i and of the p_i, which at low temperatures, when transitions between the sublevels are stopped, results in a change in overall triplet concentration compared to the situation for $\boldsymbol{B}_0 = 0$ [19,26–28]. We will refer to this

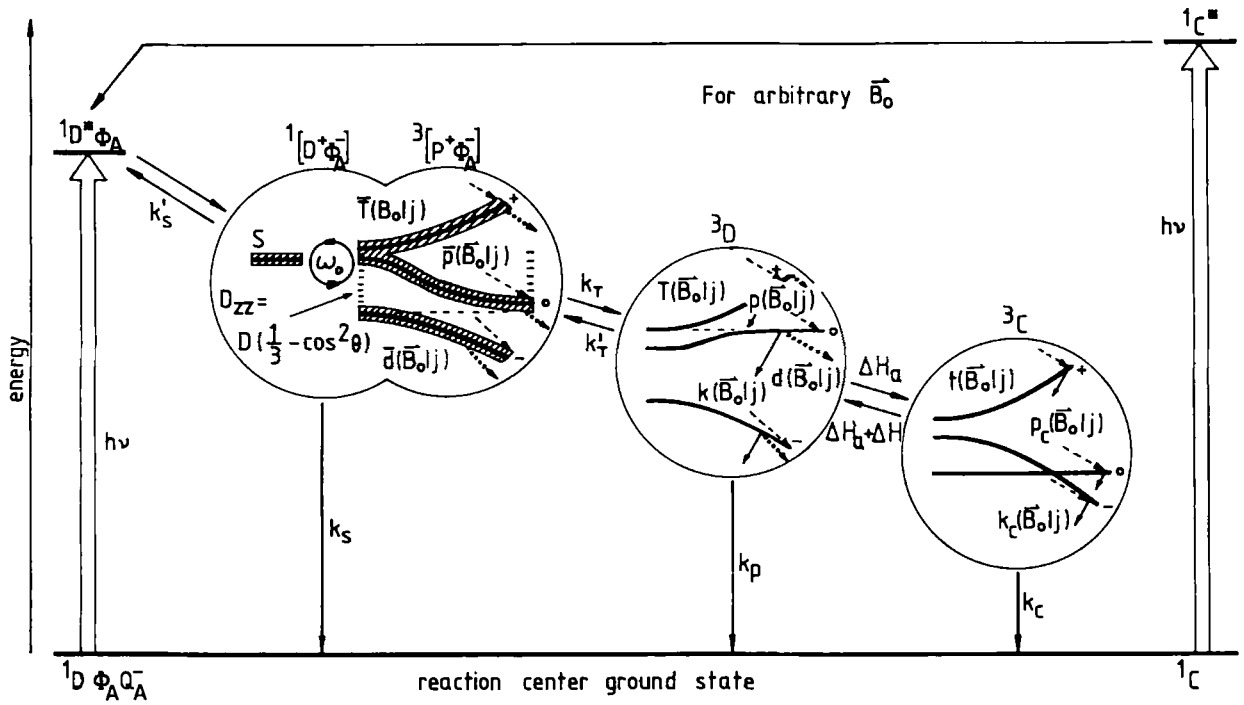

Scheme I. Energy-level scheme for the primary reactions in RC with prereduced quinone Q_A. The four circles represent the four anisotropic MFE in the RC: RPM and 3×MIMS (see text). Arrows indicate for the individual jth sublevel in field $\boldsymbol{B}_0$, ($\boldsymbol{B}_0|j$), the population probabilities p (⇢), transfer rates d (...) and decay rates k (→) of the triplet states $^3[D^+\phi_A^-]$ ($\bar{p}$, $\bar{d}$), ^3D (p, d, k) and ^3C (p_c, k_c). k_s is the rate of decay of the singlet radical pair state to the ground state, k_p the sublevel-averaged decay rate of ^3D and k_c that of ^3C. $\bar{T}$, T and t denote the triplet wavefunction of the ($\boldsymbol{B}_0|j$) sublevel in $^3[D^+\phi_A^-]$, ^3D and ^3C, respectively. The S-T mixing (frequency ω_0) of $[D^+\phi_A^-]$ mediated by hyperfine interactions is anisotropic with respect to θ, the angle between the dipolar axis of $^3[D^+\phi_A^-]$ and $\boldsymbol{B}_0$; D_{zz} is the projection of the (axial) dipolar interaction on the magnetic field. The energy levels of the radical-pair state are lifetime-broadened. The ^3D state decays partly via the $^3[D^+\phi_A^-]$ state [61] with an activation enthalpy of 0.12 eV (950 cm^{-1}).

particular MFE, as MIMS. Note that at low temperatures, not only ^3D and ^3C but also the radical pair triplet $^3[D^+\phi_A^-]$ will show a MIMS effect. The two MFEs, RPM and MIMS, for the radical pair states $^{1,3}[D^+\phi_A^-]$ and the triplet state ^3D and ^3C are summarized in Scheme I.

Both the RPM and the MIMS MFEs are anisotropic. The RPM depends on the angle θ, between the magnetic field, $\boldsymbol{B}_0$, and the z-axis of the dipolar tensor of the radical pair. MIMS depends on the relative orientation of the principal axes system (p.a.s.) of the $^3[D^+\phi_A^-]$ and ^3D triplets with respect to the laboratory frame. These anisotropies give rise to the linear dichroic MODS effect and the MODS LD-(T − S) spectrum [19]. Note that the MODS LD-(T − S) spectrum is different from the ADMR LD-(T − S) spectrum [29–31]: in LD-ADMR the angle between the optical, μ^o, and the microwave, μ^{mw}, transition moments is fixed and one averages over the angle between the $\boldsymbol{B}_1$ field and $\vec{\mu}^{mw}$, whereas in MIMS the position of μ^o in the p.a.s. is fixed and one averages over the angles of $\boldsymbol{B}_0$ with respect to the axes of the p.a.s. Thus, the two types of LD-(T − S) spectrum give different spatial information.

The present study

We have recorded MODS (T − S) spectra over the temperature range 10–288 K. From the spectra we have determined the ^3C yield as a function of temperature. We conclude that the ^3C state is in thermal equilibrium with ^3D with an activation enthalpy for D → C triplet transfer of 0.02 eV. The energy difference between ^3D and ^3C has also been determined and the mechanism of transfer is discussed.

A further result of our study is the determination of the width of the bleaching of the long-wavelength D(−) band and its shift as a function of temperature. We attribute the temperature-dependence of these two phenomena to thermal broadening of the transition and partially to expansion of the D dimer with increasing temperature.

Materials and Methods

Preparations of RCs

Cells of *Rb. sphaeroides* 2.4.1 and *R. rubrum* S1 were grown anaerobically in a medium according to the method of Cohen-Bazire et al. [32] supplied with yeast extract (5 g/l) and peptone (2 g/l). After 3–4 days of growth with incandescent lamp illumination (2 × 40 W) in a stationary culture, the cells were harvested by centrifugation.

RC of *Rb. sphaeroides* 2.4.1 were prepared essentially following the procedure given by Vadeboncoeur [33], for details see Ref. 28. Their purity is characterized by

the absorbance ratio $A_{280}/A_{802} = 1.3$. RCs of *R. rubrum* S1 were prepared following the procedure described in Refs. 34–36, for details see Ref. 28. The ratio A_{365}/A_{802} was 1.5.

For the MODS experiments the RCs were photochemically prereduced in the presence of 10 mM sodium ascorbate and diluted with ethylene glycol (67%, v/v) to an optical absorbance of 1.7 cm^{-1} at 802 nm, 293 K, to reduce the number of cracks that appeared in the sample during cooling.

Instrumental

The basic experimental apparatus is described in Ref. 18. For cooling, a helium flow system was used, while the temperature was measured with a Pt100 element that was placed inside the sample in the focussed white-light spot of the single-beam absorption spectrophotometer. This beam was quite intense (approx. 1.5 W cm^{-2}) to excite sufficient RC into the ^3D state. A sinusoidally modulated magnetic field (frequency f_m = 315 Hz) was applied perpendicular to the propagation

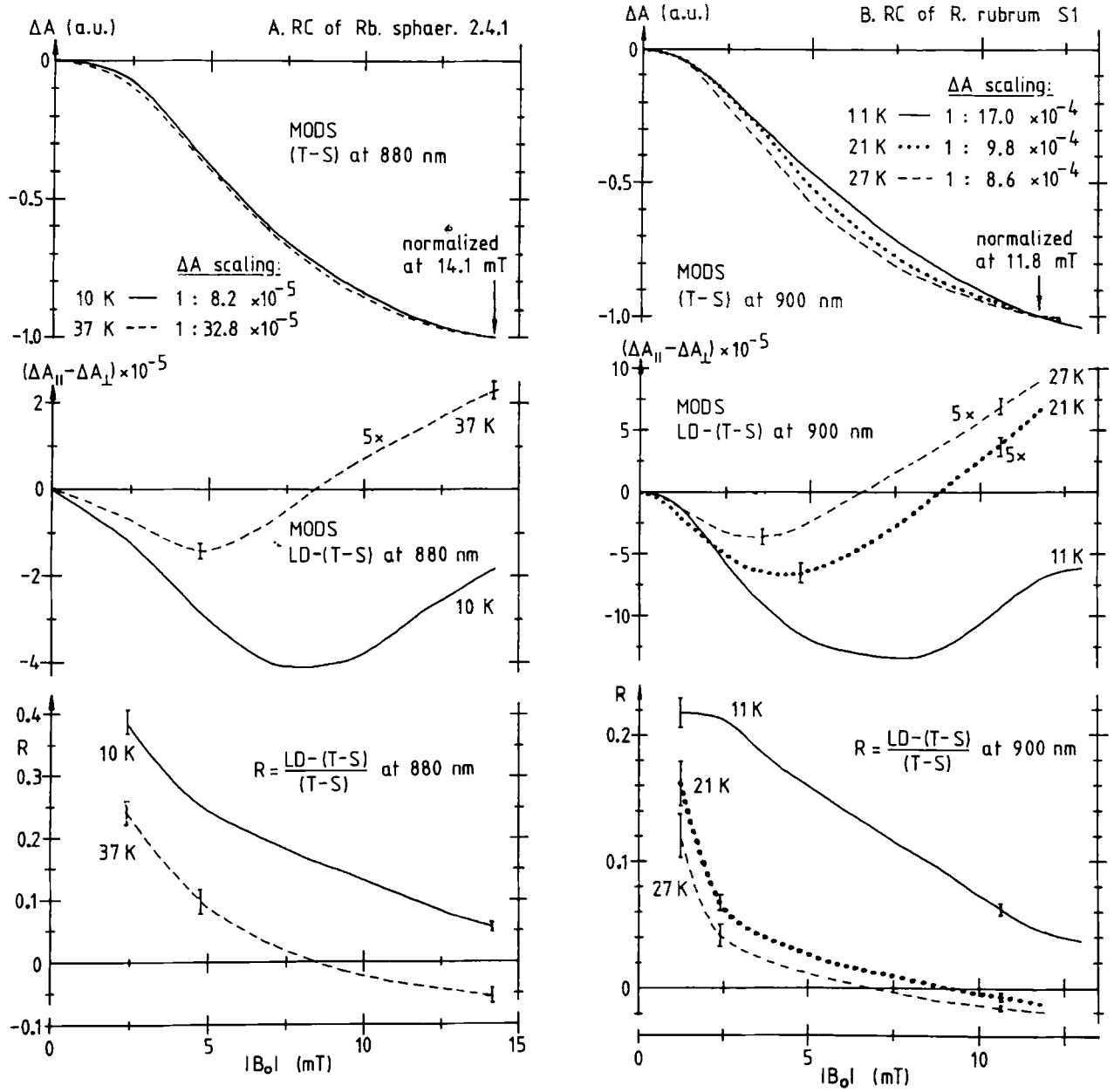

Fig. 1. LD-MODS-monitored MFE curves at several temperatures measured at the low exciton band of the primary donor, D(−), for RC of (A) *Rb. sphaeroides* 2.4.1. and (B) *R. rubrum* S1. The horizontal axis is the amplitude $|B_0|$ of the magnetic field modulation. The isotropic (T − S) traces are arbitrarily normalized at 14.1 mT (A) and 11.8 mT (B) to facilitate the comparison of the shape of the traces. Absolute scalings are indicated. Some LD-(T − S) curves are magnified five times as indicated. The bottom parts of the figures show the MFE anisotropy ratio R = LD-(T − S)/(T − S). The curves were recorded as a continuous function of $|B_0|$, error bars indicate error limits in selected parts of the curves. The optical absorbance at 802 nm was 0.2 for both preparations.

direction of the optical beam by a Helmholtz coil wrapped around the sample, in which the RC were randomly oriented. The orientation-dependent contribution of each RC produced a modulated optical anisotropy (frequency $2f_m$), which was analysed by a photo-elastic modulator at frequency $f_p = 100$ kHz in the same way as was done in our LD-ADMR experiments [29–31]. Combined phase-sensitive dectection at $2f_m$ and f_p resulted in simultaneously monitored isotropic (T − S) and anisotropic LD-(T − S) signals.

Results

The MODS-monitored MFE

In the upper parts of Fig. 1, the isotropic MODS signal intensity of *Rb. sphaeroides* 2.4.1 and *R. rubrum* S1 measured at the top of the long-wavelength absorbance band of D (the lower-energy exciton or D(−) band) as a function of $|\boldsymbol{B}_0|$ is shown for different temperatures. The MFE curves have $B_{1/2}$ values (defined as the value of $|\boldsymbol{B}_0|$ at which half the MFE is attained) of about 10.0 mT at 100 K. We have found previously for *Rb. sphaeroides* R-26 [19] that the intensity and shape of the MFE curve is increasingly determined by the MIMS effect when the temperature is lowered below 50 K. As also seen in Ref. 19, the temperature-dependence of the MIMS contribution to the MODS intensity, which follows the temperature-dependence that spin-lattice relaxation (T_1) processes have, is quite steep (Fig. 2). Between 20 and 50 K there is a transition region in which both MFE mechanisms, MIMS and the RPM, contribute to the MODS signal. Below 20 K, MIMS predominates. ^{3}D is populated via the RPM so that field-dependent differences in populating probabilities will also, via the effect of MIMS on the S–T mixing, influence the shape of the LD-MFE curve at 10 K or lower. The similarity of the curves of Fig. 1 to that for *Rb. sphaeroides* R-26 [19] points to a high degree of correlation in structure and functioning of the molecules involved in primary electron transport in the three species. An Arrhenius plot of the MODS (T − S) temperature-dependence of RC of *Rb. sphaeroides* 2.4.1 (Fig. 1A, inset) shows two straight lines with a break in the transition region at about 25 K, which reflect the two distinct temperature-dependent processes of the MFE.

Isotropic (T − S) spectra

MODS is ideally suited to study the temperature-dependence of (T − S) spectra. We have measured (T − S) spectra in the temperature range 10–288 K of RC of *Rb. sphaeroides* 2.4.1 (Fig. 3a) and *R. rubrum* S1 (Fig. 3b). The spectra are normalized at the top of the D(−) band. RC of *Rb. sphaeroides* 2.4.1 contain mainly spheroidene as carotenoid, while those of *R. rubrum* S1 have mainly spirilloxanthin [6]. The (T − S) spectra at

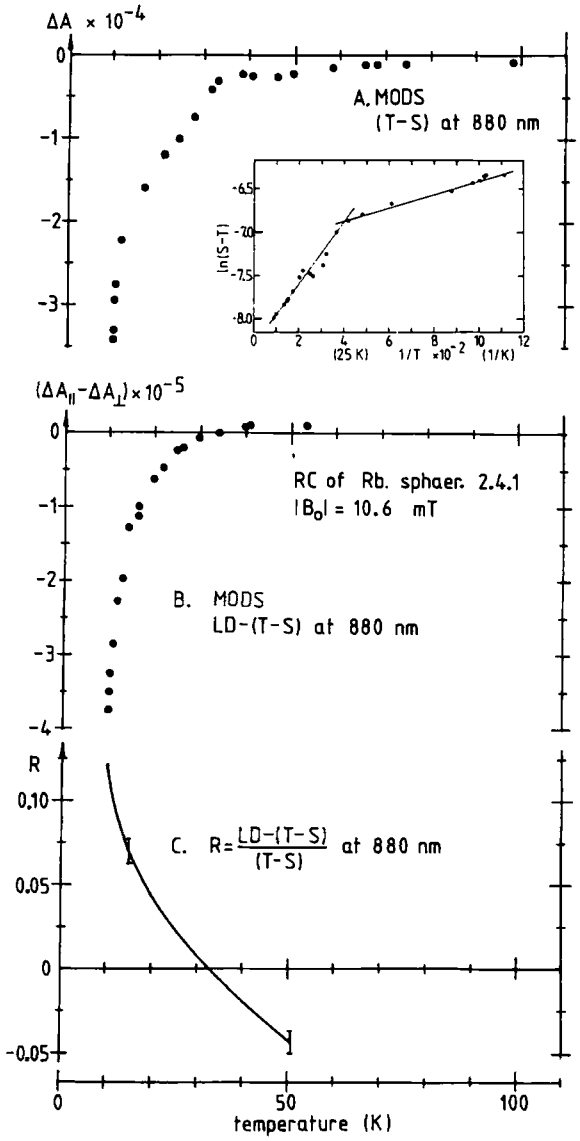

Fig. 2. Temperature-dependence of MODS (T − S) (A) and MODS LD-(T − S) (B) signals near the top of the D(−) band (880 nm) of RC of *Rb. sphaeroides* 2.4.1. (C) The anisotropic MFE ratio R = LD-(T − S)/(T − S) constructed from the traces in (A) and (B). Inset: Arrhenius plot of the amplitude of the MODS signal. Error bars indicate errors in selected parts of the curve. The spectral resolution was 4 nm and $|\boldsymbol{B}_0| = 10.6$ mT.

288 K agree very well with spectra measured through laser flash-induced kinetics by Cogdell et al. [37]. In Table I we have summarized the main features of the (T − S) spectra of both bacterial species. To facilitate comparing the spectra we have put side-by-side the features that agree with the same band assignment. The spectra of both RC types show similar temperature effects in the infrared region and in the blue region. For instance, both species show a similar linear temperature-dependence of the shift of the D(−) band to lower energy ('red shift') and a similar sharpening of this band on cooling (Fig. 4). In the blue and green regions there is almost no sharpening of bands upon

cooling. The intensities of the bands in these regions vary in harmony without changing their relative amplitudes. The increase of the T − S intensity in the spectral region of carotenoid absorption agrees with the temperature-dependent triplet transfer between dimer and carotenoid that has been found in Refs. 37 and 38. In the Discussion we will determine the ^3C yield as a function of temperature. The results will be interpreted with a model that assumes thermal equilibrium between the ^3D and ^3C states.

Anisotropic (T − S) spectra

As far as our instrumental sensitivity allowed, we have measured linear dichroic (T − S) spectra with respect to the macroscopic $\boldsymbol{B}_0$ axis. The $|\boldsymbol{B}_0|$ dependence of the MODS LD-(T − S) signals (Fig. 1) is similar to that of *Rb. sphaeroides* R-26 [19]. From the sharp increase in MODS (T − S) and MODS LD-(T − S) intensities going from 50 K to lower temperatures (Fig. 2), which is attended by a clear change in the ratio R = LD-(T − S)/(T − S), we conclude that at 10 K the MIMS effect is much larger than the RPM effect. The change in R between 10 and 50 K reflects the different preferred orientation directions of the RPM and MIMS. The shape of the curve of the MODS LD-(T − S) intensity vs. $|\boldsymbol{B}_0|$ (Fig. 1) at around 10 K is governed by the fine-structure parameters of the $^3[D^+\phi_A^-]$ and ^3D states. Between 10 and about 50 K the curves reflect increasingly the contribution of the RPM to the MFE.

Some MODS LD-(T − S) spectra are shown in Fig. 5. In the spectra of *R. rubrum* S1 no carotenoid absorption band (around 580 nm) is observed at higher temperatures where the RPM dominates. For the RPM-induced MFE, zero LD-MODS intensity results when the transition moment stands at the magic angle to the dipolar axis of $^3[D^+\phi_A^-]$. In *Rb. sphaeroides* 2.4.1, the carotenoid peak at 548 nm is clearly present. Going from low temperatures where MIMS dominates, to higher temperatures where the RPM dominates as the source of the anisotropic MFE, both species show the same sign reversal of the MODS LD-(T − S) signal in the infra-red region (Fig. 2) as was found for RC of *Rb. sphaeroides* R-26 [19]. For *Rb. sphaeroides* 2.4.1 it is striking that the carotenoid T–T absorption peak at 548 nm does not follow this reversal, despite the fact that it is populated from the ^3D state. Since the contribution to the anisotropy due to the $^3[D^+\phi_A^-] \rightarrow {}^3D$ step will be most likely the same for both species, this means that (i) at least two ^3C sublevels have different p_i/k_i ratios and (ii) the p.a.s. of ^3D and ^3C are oriented differently.

The bands in the Q_y region of the LD-MODS spectra at 10 K in Fig. 5a, b are similar to those of the LD-ADMR spectra taken at the |D|–|E| transition [30]. The relative amplitude of the 870 and 890 nm bands, however, is different, as are the amplitudes of the bands at 819 nm. These differences reflect the different selection mechanism of LD-MODS and LD-ADMR. At about 29 K, the 807 nm peak in the MODS LD-(T − S) spectra of both species is absent, while it is still strongly present in the corresponding MODS (T − S) spectra. This corresponds to the change in the origin of the MFE, i.e., MIMS at low and RPM at high temperatures, each having a different orientation-dependence.

Discussion

Isotropic (T − S) spectra

We will first focus on the wavelength region below 650 nm, then on that above 650 nm, whereafter we will discuss the temperature effects on the D(−) band.

Below 650 nm. In the blue region, D and the accessory BChl and BPh have S–S transitions at about 360–385 nm (B_x and B_y bands), while those of the

TABLE I

Features and assignments of the (T − S) spectra of Fig. 3 of RC of Rb. spaeroides 2.4.1 and R. rubrum S1

t−, negative band; t+, positive band; sh, shoulder; S–S, singlet–singlet absorption; T–T, triplet–triplet absorption; bl, bleaching upon triplet formation.

Reaction centers of				Assignment
Rb. sphaeroides 2.4.1		*R. rubrum* S1		
λ(T − S)		λ(T − S)		
355	t+/sh			BChl, (S–S) bl
372	sh	385	sh	BChl, (S–S) bl
381–390	t+	400	t−	
401	t+	419	sh	(T–T) of ^3C
416	t+	431	t+	(T–T) of ^3C
430	t+	445	sh	
450–458	sh	478	t−	^1C, (S–S) bl
472	t−	502	sh	^1C, (S–S) bl
500	sh	538	sh	^3C, (T–T) + ^1C, (S–S), bl
520	sh	572	sh	^3C, (T–T)
544–548	t+	589	t+	
572	t+	603	t+	
602	t−	600	t−	Q_x, (S–S) of BChl and BPh, bl
605	sh	607	sh	
624	t+	631	t+	(S–S), higher vibrational states of Q_y of BChl and BPh
654	t−	659	t−	
680	sh	680	sh	
690	t+	690	t+	
701	sh	706	sh/t+	
722	t−	730	t−/sh	
753	t+	753	t+	coupled μ^0 of Q_y of BPh
772	t+	770	t+	
793	t+	795	t+	exciton coupled μ^0 of Q_y of BChl
800	t−	801	t−	
807	t+	807	t+	
813	t−	813	t−	
819	t+	819	t+	
848–882	t−	862–896	t−	Q_y, (S–S), D(−) band

carotenoids lie between 430 and 550 nm. These bands show up with negative sign (as 'bleachings') in the (T − S) spectra when ^{3}D or ^{3}C is formed in the RC. With positive sign, bands will appear that can be ascribed to T–T electronic transitions of ^{3}D and ^{3}C and to S–S transitions of neighboring molecules (BChl and/or BPh) that are excitonically coupled via electric dipole–dipole interaction to D and C, and therefore will redistribute their intensities, energies and orientation in the RC upon triplet formation. All these effects overlap strongly in this region. Following Bensasson et al. [39], we ascribe the peaks at 548 nm for *Rb. sphaeroides* 2.4.1 and at 589 nm for *R. rubrum* S1 to T–T absorption of ^{3}C, assuming a temperature-independent 30–38 nm red-shift of their in vitro values that is presumably caused by the interaction of carotenoid with its environment. At each side of these peaks overlapping bands are present that are similar to the S–S absorption peaks of in vitro carotenoids [7,40] and probably represent three vibrational overtones.

The changes in the 350–400 nm region are probably due to the effect of ^{3}C formation on the S–S transitions of B_B and ϕ_B, as the temperature-induced changes in intensity of the 372 and 381–390 nm peaks in *Rb. sphaeroides* 2.4.1 and of the 385 and 400 nm peaks in *R. rubrum* S1 are in harmony with those of the T–T peaks at 548 and 589 nm, respectively. The observed bands cannot be due to strong excitonic coupling between D and C, because at 10 K the B_x, B_y and Q_x, Q_y bleachings of D due to ^{3}D formation do not induce absorbance changes of the (S_n–S) bands of C.

In the (T − S) spectra at 10 K, shoulders at 605 and 607 nm are resolved in the Q_x band bleaching at 602 and 600 nm for *Rb. sphaeroides* 2.4.1 and *R. rubrum* S1,

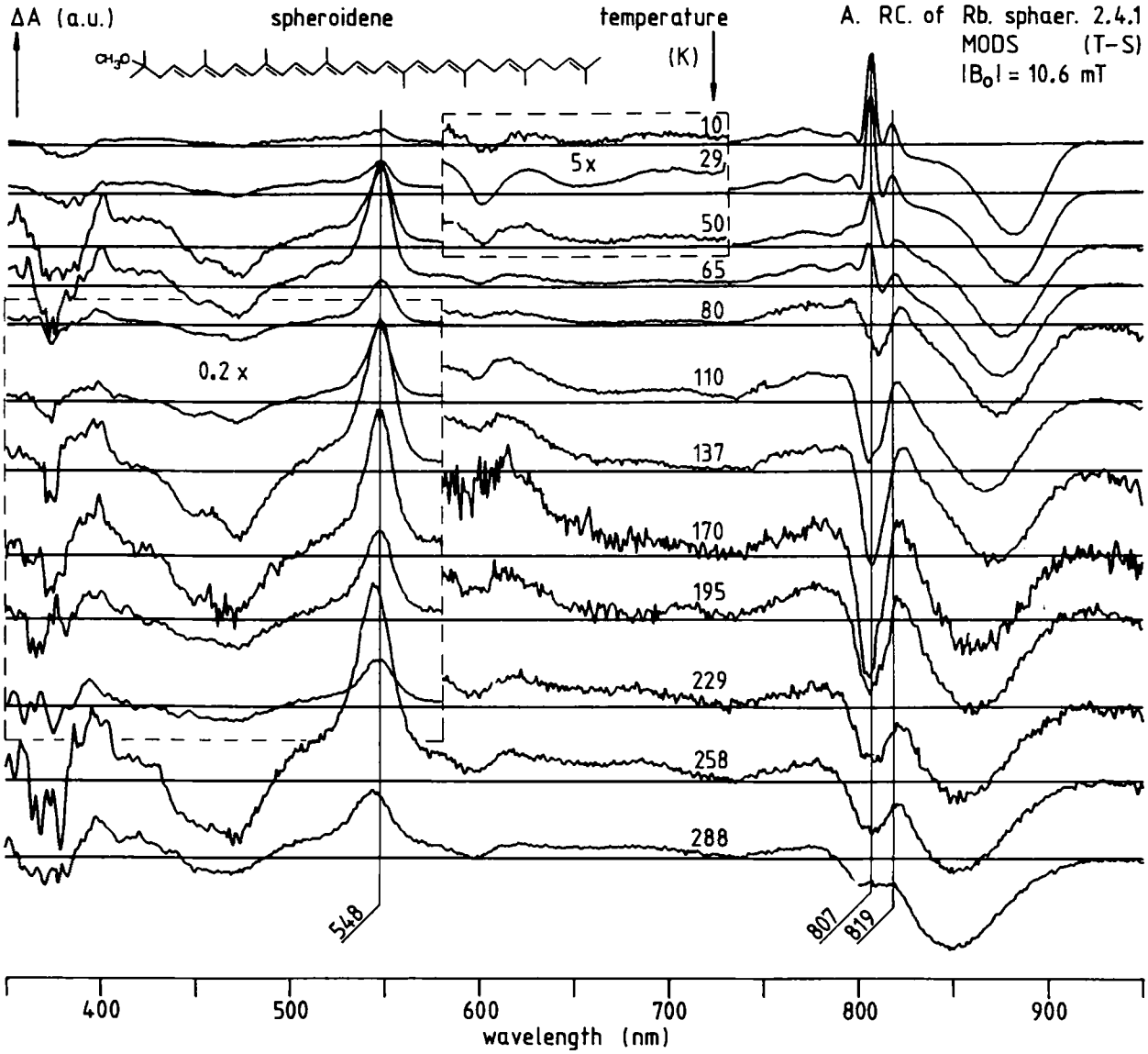

Fig. 3. MODS (T − S) spectra at various temperatures of RC of (A) *Rb. sphaeroides* 2.4.1 and (B) *R. rubrum* S1, normalized on the amplitude at the top of the D(−) band between 850 and 900 nm. Spectral resolution was 3.2 and 2.4 nm, respectively. Note the different vertical scale in some parts of the figure framed by a broken line.

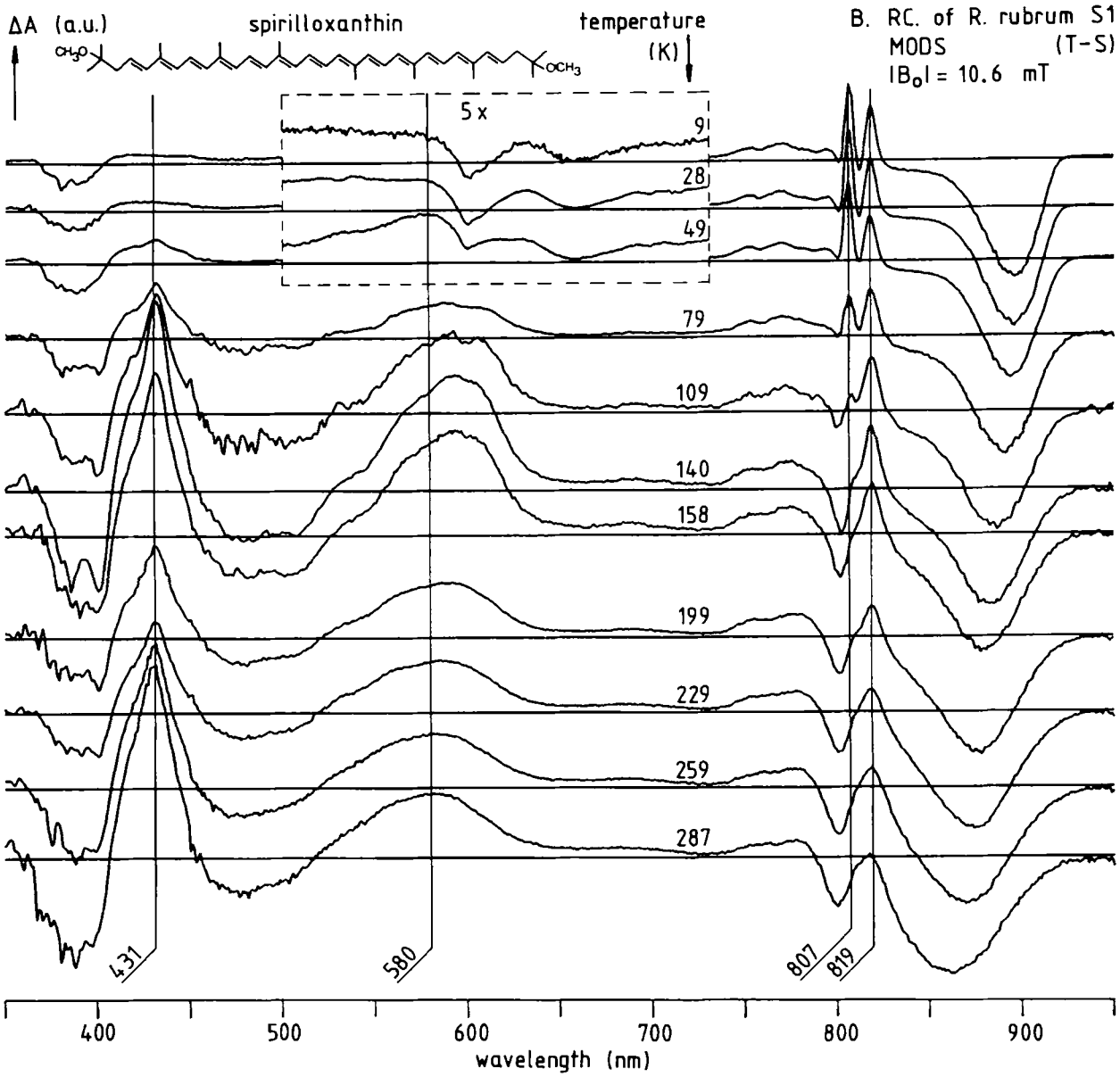

Fig. 3 (continued).

respectively (Table I). The top of the peak belongs to the Q_x of D [41], while the shoulder is ascribed to a ^{3}D-induced absorbance change of the adjacent accessory BChl molecules.

Above 650 nm. Calculations based on the RC structure of *Rhodopseudomonas viridis* [31,42] indicate that the Q_y of the BChl have electric dipolar interactions in the order of 100–1000 cm^{-1}. This is the reason why when ^{3}D is formed, the dimeric exciton bands D(+), D(−) disappear and a new composition of transition moments of the BChl and BPh is formed. Since the widths of the Q_y bands narrow upon cooling (up to a factor of approx. 2 for the D(−) band in the temperature range studied) sharp features show up at low temperatures. The Q_x, B_x and B_y bands do not show this temperature effect on their bandwidth. Note that the MODS-recorded bleaching of the D(−) band represents the full band of the singlet ground state spectrum. This contrasts with the bleaching of the D(−) band in the ADMR-recorded (T − S) spectrum, which is somewhat narrowed because of site-selection effects [29,30].

The peaks at 819 and approx. 795 nm show for both species comparable, relatively small changes in intensity and band position as a function of the temperature. In contrast, the peak at 807 nm is strongly temperature-dependent and has practically disappeared at the same temperature (140–160 K) at which the intensities of the T–T peaks of C are maximal, as is most clearly observed in Fig. 3a. The transition moment μ^0 of the 807 nm band is largely composed of contributions of the accessory BChl and the singlet component of the partly localized ^{3}D state. Admitting that C is located at the B

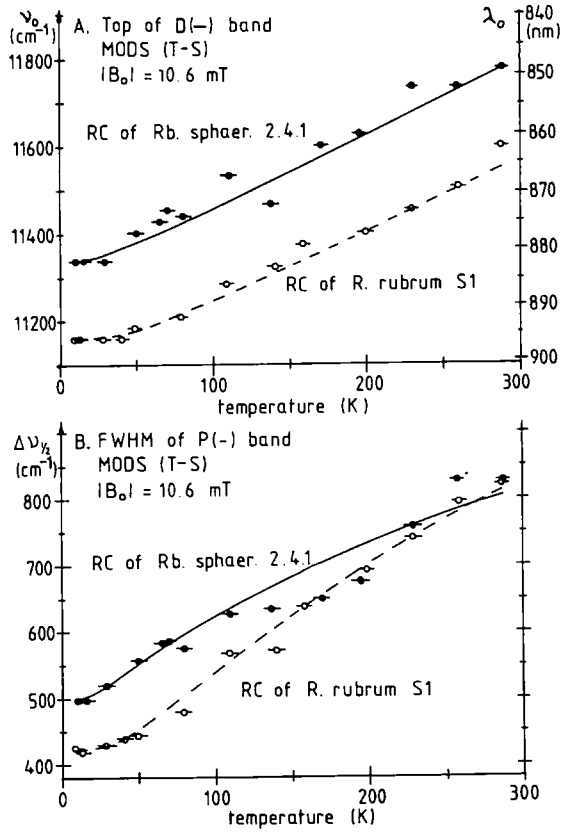

Fig. 4. Peak position (A) and width (B) of the D(−) band of RC of *Rb. spaeroides* 2.4.1 (filled symbols) and *R. rubrum* S1 (open symbols) as a function of the temperature. Data from Fig. 3. No attempt was made to correct for the spectral overlap at the high-energy side of the D(−) band. The lines are simulations according to Eqns. 1 and 2 with the parameters given in Table III.

side of D, the strong bleaching of the 807 nm band appears to be caused by the ^{3}C state, whose triplet wavefunction is partly spread over B_B.

The 807 nm peak in (T − S) spectra of RC of the carotenoidless mutant *Rb. sphaeroides* R-26 decreases much more smoothly and monotonically than that of the wild-type [18,19]. In this case, no triplet character is mediated to B_B and the temperature behavior of the intensities of the peaks at 795, 807 and 819 nm can be explained by band broadening and an increased delocalization of the triplet exciton over the BChl of the D dimer with increasing temperature. These latter effects are also present in *Rb. sphaeroides* 2.4.1 and *R. rubrum* S1. For RC of *Rps. viridis*, where transfer of triplet excitation from ^{3}D to C does not take place [43,44], we have observed that the 838 nm band (the analogue of the 807 nm band of *Rb. sphaeroides* R-26) decreases little in intensity and remains resolved in the temperature range from 1.2 to 300 K [17,44]. The triplet localization on this dimer is apparently not drastically altered in this temperature range.

In the region between 680 and 730 nm some small reproducible absorbance changes are visible. We assume that these absorbance differences originate from shifts in higher vibrational states of the Q_y of the BChl due to ^{3}D formation.

The 10 K spectra show only small absorbance changes of the BPh between 730 and 780 nm, which confirms the small excitonic coupling between the BChl of D and the BPh previously found [31,42,45].

Temperature effects on the D(−) band. Plotting the peak position and the width of the D(−) band versus temperature results in nearly straight lines at temperatures above 50 K (Fig. 4). Similar results were obtained by Kirmaier et al. [46,47], who found for the width and peak position of the D(−) band of *Rb. sphaeroides* 2.4.1 the same relative change as function of the temperature. The red-shift of the D(−) band upon cooling could be due to contraction of the protein environment around D. Because of the short center-to-center distance of the dimer with respect to other interpigment distances, the exciton interaction between the dimer components is by far the strongest, and is to a large extent responsible for the red-shift of the D(−) band at ambient temperatures compared to the in vitro BChl Q_y absorption. Since the change in the dipolar coupling is proportional to r^{-3}, with r the distance between the RC pigments, contraction by cooling will affect the dimer–exciton interaction, and thus the D(−) band position, much more than that of the other pigments, For example, a displacement of one of the accessory BChl of 0.3 Å at $r = 10$ Å causes an energy shift of 1 nm (16 cm^{-1}) at 800 nm, while for D(−) with $r = 3$ Å a 1 nm (13 cm^{-1}) shift at 890 nm requires a displacement of a dimer-BChl of only 0.01 Å.

Contraction influences both the kinetics of electron transport and the energy of the D(−) band as evidenced by the effects of isotropic pressure. Hoganson et al. [48] found that isotropic pressure increased the recombination rate of $D^+Q_A^-$, whereas Clayton and Devault [49] observed at 6000 atm a red-shift of the D(−) band of 29 nm (380 cm^{-1}) at 300 K.

The rate constant of charge separation k_{cs} as given by the theory of electron transfer is proportional to the magnetic exchange coupling $|J|$ between D^+ and ϕ_A^- [50,51], which depends exponentially on the distance r between D and ϕ_A by $k_{cs} \propto |J| \propto \exp(-2 \cdot 6r)$. Martin et al. found that charge separation occurs in 2.8 ps at 300 K [4] and in 1.2 ps at 10 K [52]. This increase of the rate of charge separation can be fully accounted for by a contraction of the protein induced by cooling, leading to a shortening of the distance between D and ϕ_A by $\Delta r = 0.33$ Å. Assuming a homogeneous contraction of the RC, the D-B_A or D-B_B and the D_A-D_B distances will then be shortened by about 0.2 Å and 0.07 Å, respectively, and will induce band-shifts of about 0.6 and 7 nm, respectively. Since the cooling-induced band-shift of D(−) is about 34 nm for both species, we conclude that contraction can only partly explain this shift.

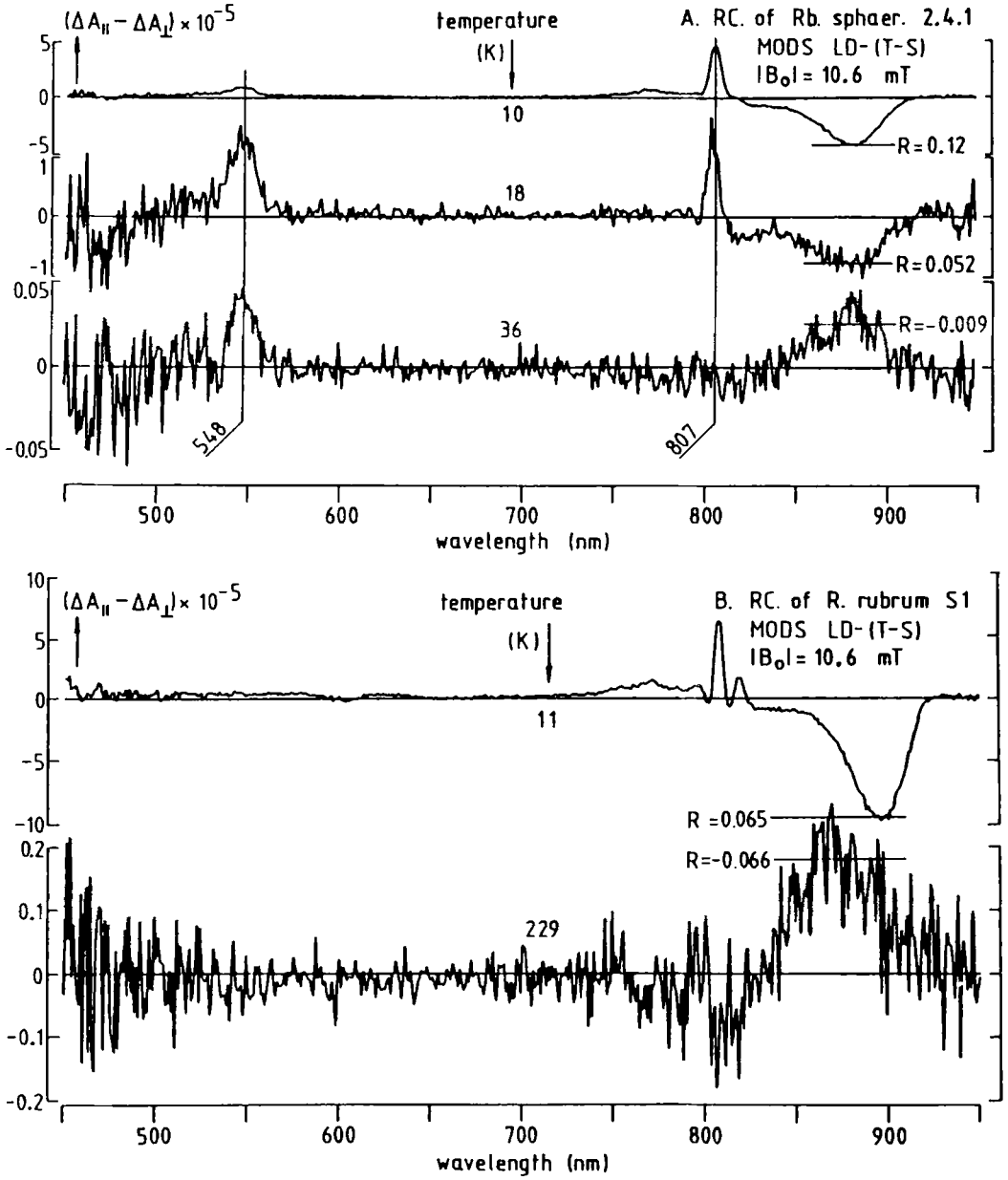

Fig. 5. Some of the LD-(T − S) spectra monitored with the LD-MODS technique simultaneously with the spectra of Fig. 3. Amplitudes and R values correspond to Figs. 1 and 2. (A) RC of *Rb. spaeroides* 2.4.1. In the temperature range 36–110 K the spectra were similar to the 36 K spectrum with respect to the signal-to-noise ratio and peak ratio of the amplitude at 548 nm to that of the D(−) band, and are therefore not displayed. As for *Rb. spaeroides* R-26 [19] the R value was constant above 50 K. (B) *R. rubrum* S1; similar spectra as the 229 K spectrum were found between 40 and 288 K (see (A)).

Hole-burning experiments have shown that the D(−) band is mainly lifetime broadened [53,54]. This means that the D(−) bandwidth should increase with decreasing temperature if it is fully determined by the lifetime. We observe an opposite effect, so that at 288 K an appreciable part of the D(−) band must be vibrationally broadened, showing at 300 K a relatively strong bleaching in the 800 nm region.

Scherer et al. [55] attempted to explain the temperature-dependent red-shift of D(−) with a model in which the vibrational motion of the atoms of the dimer D is coupled to the dipolar interaction between D_A and D_B. Our attempt to fit both the temperature-dependence of the maximum of the D(−) band and that of its width with the formulae of Ref. 55 and one set of parameters was unsuccessful, possibly due to the neglect in Ref. 55 of contraction effects.

Recently Hayes et al. [56] have described thermal effects on the bandwidth, $\Delta\nu_{1/2}$ (in cm^{-1}) of D(−) by the theory of electron–phonon coupling:

$$(\Delta\nu_{1/2,\mathrm{inhom}})^2 = S(\hbar\omega_m)^2 \coth(\hbar\omega_m/2k_BT) \quad (1)$$

where $\Delta\nu_{1/2,\mathrm{inhom}}$ is the inhomogeneous linewidth, S the

TABLE II

The parameters of Eqn. 6 used in the fits of the $[^3C]/[^3D]$ ratio as a function of the temperature shown in Fig. 6

	Rb. sphaeroides 2.4.1; curve:			*R. rubrum* S1; curve:		
	1	2	3	1	2	3
k_1^0/k_2^0	0.0394	0.0080	0.8342	0.0698	0.1189	$0.1282 \cdot 10^{-7}$
k_3/k_2^0	$0.18 \cdot 10^{-3}$	$0.50 \cdot 10^{-4}$	$0.41 \cdot 10^{-2}$	$0.47 \cdot 10^{-2}$	$0.74 \cdot 10^{-2}$	$0.13 \cdot 10^{-8}$
ΔH_a (eV)	0.022	0.019	0.020	0.020	0.020	0.017
ΔH (eV)	0.115	0.145	0.060	0.060	0.050	0.280
For $k_3 = 7.7 \cdot 10^4$ s^{-1}:						
k_1^0 (s^{-1})	$1.7 \cdot 10^7$	$1.2 \cdot 10^7$	$1.6 \cdot 10^7$	$1.2 \cdot 10^6$	$1.2 \cdot 10^6$	$7.5 \cdot 10^5$
k_2^0 (s^{-1})	$4.3 \cdot 10^8$	$1.6 \cdot 10^9$	$1.9 \cdot 10^7$	$1.6 \cdot 10^7$	$1.0 \cdot 10^7$	$5.9 \cdot 10^{13}$

$\Delta\epsilon(^3D-D) = \Delta\epsilon(D^+-D) = 100000$ $M^{-1} \cdot cm^{-1}$ at 860 nm for BChl *a* [a]
$\Delta\epsilon(^3C-C) = 43000$ $M^{-1} \cdot cm^{-1}$ at 580 nm for spirilloxanthin (*R. rubrum* S1) [39]
$\Delta\epsilon(^3C-C) = 29000$ $M^{-1} \cdot cm^{-1}$ at 540 nm for spheroidene (*Rb. spaeroides* 2.4.1) [39]

[a] In view of the uncertainties in the determination of $\Delta\epsilon(^3D-D)$ we have assumed that the differential molar absorption coefficient of oxidized D, D^+, with respect to the ^1D ground state is a good approximation for that of ^3D with respect to ^1D and have chosen for both species $\Delta\epsilon(D^+-D) = 100000$ $M^{-1} \cdot cm^{-1}$ [57,58,72].

Huang-Rhys factor (a measure of the strength of electron–phonon coupling) and ω_m the mean phonon frequency. The position of the D(−) band, ν_0 (in cm^{-1}), depends on the effect of temperature on both the thermal vibration of, and the mean distance between, the two BChl of D. We have adjusted the equation of Scherer et al. [55] for ν_0:

$$\nu_0 = a + b \coth(\hbar\omega_m / 2k_B T) \quad (2)$$

by taking the constants a and b as freely adjustable parameters to take into account the effect of contraction. We have used Eqns. 1 and 2 to make fits to the data of the RC of *Rb. sphaeroides* 2.4.1 and of *R. rubrum* S1 (drawn and broken lines in Fig. 4). The parameters used are given in Table III. We have assumed the temperature-dependence of ω_m to be negligibly small and have also confined the number of fit parameters by making ω_m equal in both Eqns. 1 and 2. (Somewhat better fits can be obtained by changing ω_m and b by 20% in fitting ν_0, compared to the values for the linewidth.) Nevertheless, the values resulting from these simulations (Table III) are within the same range as those found by Hayes et al. [56] from a fit to hole-burning spectra of *Rb. sphaeroides* R-26, *Rps. viridis* and Photosystem I of plants, with the exception of our Huang-Rhys factor, which is about 2.5–3-times larger than that of Hayes et al. This points to a stronger electron–phonon coupling for the RC studied by us.

We have previously found for *Rb. sphaeroides* R-26 [18,19] that when the area of the D(−) band is normalized at each temperature, an approximate isosbestic point is observed at which wavelength the absorption remains constant during cooling. Therefore, the shift in the D(−) peak position was interpreted in Refs. 18 and 19 to result from a temperature-dependent equilibrium between two stable configurations of the dimer with a somewhat different D(−) absorption. For the carotenoid-containing RCs of the present work no such isosbestic point was found. In these RCs the presence of a carotenoid may influence the equilibrium between the two proposed conformations of the dimer so that one conformation is favored. In the absence of carotenoid, the BChl dimer of D may have more room in the RC protein to move into another position.

In the next sections we will discuss our study of the ratio of the ^3C and ^3D concentrations. Differences between the two species with respect to the functional properties of their carotenoid will then become apparent.

Transfer of triplet excitation between D and C

In studying the $D \rightleftarrows C$ triplet transfer we need to eliminate the intrinsic temperature-dependence of the

TABLE III

The parameters (in cm^{-1}) of Eqns. 1 and 2 used in the fits of the bandwidth, $\Delta\nu_{1/2}$, and the energy shift, ν_0, of the D(−) band as a function of the temperature (Fig. 4)

	$\Delta\nu_{1/2,inhom}$	S	$\hbar\omega_m$	a	b
Rb. sphaeroides 2.4.1	355	12	42	11287	51
R. rubrum S1	100	15	83	11061	100

^{3}D concentration (i.e., other than that caused by D $\rightleftarrows$ C triplet transfer). This is done by determining at each temperature the ^{3}C concentration relative to the ^{3}D concentration, i.e., the ratio $[^3C]/[^3D]$. At each temperature this ratio is equal to the ratio $[\Delta^3C]/[\Delta^3D]$, where Δ stands for the MFE-induced change in triplet concentration. $[\Delta^3C]$ is given by $\Delta A_{car}/(\Delta\epsilon_{car} \cdot l)$ were ΔA_{car} is the MFE-induced change in absorbance at the carotenoid absorption peak (548 and 580 nm for *Rb. sphaeroides* and *R. rubrum*, respectively), $\Delta\epsilon_{car}$ the differential absorption coefficient for $C \rightarrow {}^3C$ formation (Table II) and l the optical pathlength. $[\Delta^3D]$ is more difficult to determine directly, since the differential molar absorption coefficient, $\Delta\epsilon$, of the maximum of the bleaching of the D(−) band is only determined at 300 K, where it is 112 000 $M^{-1} \cdot cm^{-1}$ for *Rb. sphaeroides* R-26 [57] and 90 000 $M^{-1} \cdot cm^{-1}$ for *Rb. rubrum* S1 [58]. On cooling, there is an appreciable shift and change in line-shape of the D(−) band (Fig. 3). The dipole strength of the D(−) band, however, is approximately temperature-independent. Clayton and Yamamoto [59] have measured the absorbance spectrum of RC of *Rb. sphaeroides* R-26 at 300 and 35 K. Allowing for the asymmetric shape of the (D−) band at low temperature [30], the dipole strengths of D(−) at 300 and 35 K agree to within 5% (measured on the spectrum of Fig. 2 of Ref. 59 which was enlarged 6-fold and converted to cm^{-1} abscissa). We may therefore use the definition of the dipole strength of the D(−) transition to evaluate $[\Delta^3D]$:

$$|\vec{\mu}^0|^2 = 9.180 \cdot 10^{-3} \int_{\substack{D(-)\\band}} (\epsilon_D/\nu)\, d\nu$$

$$= 9.180 \cdot 10^{-3} (c \cdot l)^{-1} \int_{\substack{D(-)\\band}} (A/\nu)\, d\nu \qquad (3)$$

where $\vec{\mu}^0$ is the optical transition dipole moment, ϵ_D the molar absorption coefficient of the D(−) band, ν the frequency, c the concentration of the RC and A the absorbance of the singlet absorbance spectrum at 288 K. Since by definition $A = \epsilon_D \cdot c \cdot l$, we may substitute for A and c, ΔA and $[\Delta^3D]$, respectively, if we take for ϵ_D, $\Delta\epsilon_D$, the differential molar absorption coefficient for $D \rightarrow {}^3D$ formation. To a good approximation, $\epsilon_D = \Delta\epsilon_D$, so that we obtain

$$\frac{[\Delta^3C]}{[\Delta^3D]} = \frac{\Delta A_{car}}{\Delta\epsilon_{car} \cdot l} \cdot \frac{l \cdot \int (\epsilon_D/\nu)\, d\nu}{\int (A/\nu)\, d\nu} = \frac{\int (\epsilon_D/\nu)\, d\nu}{\Delta\epsilon_{car}} \cdot \frac{\Delta A_{car}}{\int (A/\nu)\, d\nu}$$

$$= \frac{\epsilon_D}{\epsilon_{car}} \cdot \frac{\Delta\nu}{\nu_0} \cdot \Delta A_{car} / \int (\Delta A/\nu)\, d\nu \qquad (4)$$

where the integrals are over the D(−) band and $\Delta\nu = \Delta\nu_{1/2}\sqrt{\{\pi/(4 \ln 2)\}}$, with $\Delta\nu_{1/2}$ the full width at half-maximum of the Gaussian absorption band with center frequency ν_0 by which we have approximated the D(−) band at 288 K. Using the values given in Table II and Fig. 4, we find for the factor $(\epsilon_D \cdot \Delta\nu)/(\epsilon_{car} \cdot \nu_0)$ in Eqn. 4 at the T–T absorption peak of carotenoid, 0.24 for *Rb. sphaeroides* 2.4.1 and 0.19 for *R. rubrum* S1. The Gaussian approximation yields for the dipole strengths of the D(−) band, at 288 K, 64 and 73 D^2 for *Rb. sphaeroides* 2.4.1 and *R. rubrum* S1, respectively, in good agreement with the dipole strength reported for *Rb. sphaeroides* R-26 [60]. With ΔA_{car} and $\int_{\substack{D(-)\\band}} (\Delta A/\nu)\, d\nu$ evaluated from the spectra of Fig. 3 we have plotted the ratio $[^3C]/[^3D]$ in Fig. 6 as a function of the temperature.

$$^3D \underset{k_2}{\overset{k_1}{\rightleftharpoons}} {}^3C \xrightarrow{k_3} {}^1C$$

Scheme II. The equilibrium model for triplet transfer between D and C in the RC.

A theoretical expression for the concentration ratio of Eqn. 4 may be derived with a simple model in which it is assumed that there is an equilibrium between ^{3}D and ^{3}C with rate constants k_1 and k_2, which are temperature-dependent with activation enthalpies ΔH_a and $(\Delta H_a + \Delta H)$, respectively (Scheme II and insets of Fig. 6). ΔH is the enthalpy difference between the lowest energy levels of ^{3}D and ^{3}C. Direct decay of ^{3}C to C with rate constant k_3 is assumed to be temperature-independent, while part of the ^{3}C decay is assumed to occur via ^{3}D and is therefore temperature-dependent, see Schenck et al. [38]. We thus have

$$k_1 = k_1^0 \exp(-\Delta H_a/k_B T) \qquad (5)$$

$$k_2 = k_2^0 \exp(-(\Delta H_a + \Delta H)/k_B T) \qquad (6)$$

Keeping the ^{3}D concentration constant the change in time of the ^{3}C concentration is given by:

$$\frac{d[^3C]}{dt} = k_1 \cdot [^3D] - (k_2 + k_3) \cdot [^3C] \qquad (7)$$

The steady-state solution of Eqn. 7 yields:

$$\frac{[^3C]}{[^3D]} = \frac{k_1^0}{k_2^0} \cdot \frac{\exp(-\Delta H_a/k_B T)}{k_3/k_2^0 + \exp(-\Delta H_a/k_B T) \exp(-\Delta H/k_B T)} \qquad (8)$$

where we have assumed that the modulation frequency of the magnetic field is much lower than the inverse lifetime of ^{3}C.

Simulations according to Eqn. 8 using a four-parameter least-square fitting procedure with (k_1^0/k_2^0), (k_3/k_2^0), ΔH_a and ΔH as parameters, resulted in the fits shown in Fig. 6, using the values given in Table II. Cogdell et al. [37] and Schenck et al. [38] have found for

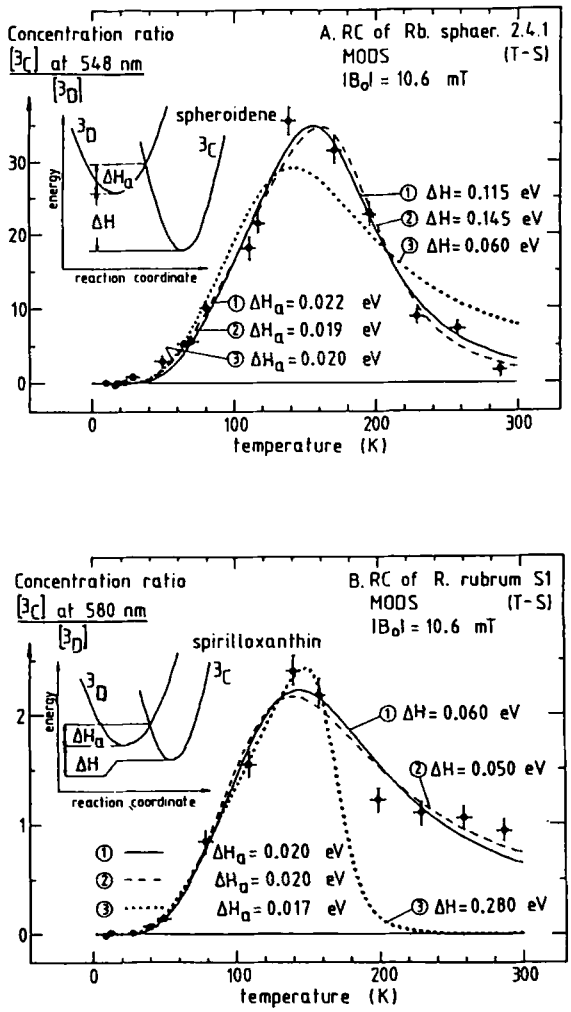

Fig. 6. Temperature-dependence of triplet transfer between D and C in RC of (A) *Rb. spaeroides* 2.4.1 and (B) *R. rubrum* S1. The data points are taken from Fig. 3 as explained in the text. The curves are fits (see text) with the parameters given in Table II. The curves labeled '1' represent the best least-squares fit. Insets: one-dimensional representation of the potential surfaces of ^{3}D and ^{3}C.

the decay time of ^{3}C values in the range 2–18 μs ($(0.55–5.0)\cdot 10^5$ s^{-1}) in the temperature range 5–300 K. This variation in decay rate is to be expected, since the decay of ^{3}C will depend on the decay of ^{3}D and the ^{3}D-^{3}C equilibrium, which are both temperature-dependent [38,61]. Taking for the temperature-independent $^3\text{C} \rightarrow {}^1\text{C}$ transition rate k_3 the decay rate of ^{3}C at the lowest temperature reported, at 5 K, $k_3 = 7.7\cdot 10^4$ s^{-1} (13 μs) [38] and we find for the temperature-independent prefactors $k_1^0 = (1.5 \pm 0.3)\cdot 10^7$ and $(1.0 \pm 0.3)\cdot 10^6$ s^{-1}, and k_2^0 = approx. 10^9 and approx. 10^7 s^{-1} for *Rb. sphaeroides* 2.4.1 and *R. rubrum* S1, respectively. The activation enthalpy $\Delta H_a = 0.020 \pm 0.005$ eV (160 cm^{-1}) is similar in both species.

We find an optimum in ^{3}C formation at 140 K, in contrast to Schenck et al. [38] who have found an optimum in ^{3}C concentration at 60 K. This lower value appears to result from a neglect of the change in ^{3}D concentration with temperature in Ref. 38. Dividing the (T − S) signal at 547 nm as a function of the temperature (Fig. 3a of Ref. 38) by the ^{3}D yield as a function of the temperature (Fig. 6c of Ref. 38), gives a curve very similar to our Fig. 6a, with a maximum at 120 K. Earlier, the ratio [^{3}C]/[^{3}D] was reported to be constant between 35 and 100 K [62]. Fig. 6 clearly shows this is not the case.

The accuracy of our determination of ΔH_a is quite high, since ΔH_a determines the smooth, low-temperature flank of the curves of Fig. 6. The high-temperature flank, on the other hand, is dominated by ΔH. Schenck et al. using their model have found 0.025 ± 0.005 eV as the activation enthalpy to the intermediate state [42], in good agreement with our result. Frank et al. [62] have reported $\Delta H \approx 0.01$ eV between 30 and 60 K, which deviates substantially from the values found by us and those in Ref. 38. This too low value of ΔH probably resulted from the short temperature interval studied in Ref. 62 and the neglect of the change in ^{3}D concentration with temperature.

The energy difference ΔE between the ^{3}D and ^{3}C levels resulting from our fits is (neglecting volume changes) 0.13 ± 0.02 eV (1050 cm^{-1}) for *Rb. sphaeroides* 2.4.1 and 0.06 ± 0.01 eV (485 cm^{-1}) for *R. rubrum* S1. This means that at 288 K the triplet transfer from ^{3}D to C is less efficient for *R. rubrum* S1 than for *Rb. sphaeroides* 2.4.1. The fit to Fig. 6a (*Rb. sphaeroides* 2.4.1) is quite unique, and since the ^{3}D energy level is at about 0.94 eV [63], the ^{3}C level is lower by ΔE at 0.81 eV. The latter agrees very well with the calculated value for ^{3}C in vitro, i.e., 0.81 eV [39]. The fit to the ^{3}C-yield curve of *R. rubrum* S1 is somewhat less good at higher temperatures. The high-temperature flank in Fig. 6b could not be reproduced exactly. An attempt to improve the fit of this flank by taking the ^{3}C decay rate k_3 temperature dependent failed, since at high temperatures k_3 presumably becomes larger, which makes the high-temperature flank even steeper.

In Figs. 6a and b we also show the sensitivity of the fits to the parameter values. In both figures the optimal fits are given by curve 1. Curve 3 of Fig. 6b shows the optimal fit in the case when ΔH was fixed at $\Delta H = 0.28$ eV, the energy difference between the in vitro triplet energy of spirilloxanthin (0.65 eV [39]) and that of ^{3}D [64]. The k_2^0 value is in this case much larger compared to the k_2^0 values of the curves 1 and 2, and in addition the fit is bad so that we reject the high value of $\Delta H = 0.28$ eV for *R. rubrum* S1. For comparison, we have taken for curve 3 in Fig. 6a for *Rb. sphaeroides* 2.4.1 the relatively low value for ΔH that was found in the optimal fit for *R. rubrum* S1 (Fig. 6b, curve 1) and calculated a best fit. Especially at the right flank the fit is poor, so that we conclude that the difference in ΔH between the two species is significant. Thus, again neglecting volume changes, $\Delta E = 0.06$ eV for *R. rubrum*

S1 and the in vivo triplet energy of spirilloxanthin is 0.88 eV (7095 cm^{-1}) above its RC ground state. This deviates from the in vitro triplet energy of this carotenoid, which was estimated to be 0.65 eV [39]. Apparently, in contrast to RC of *Rb. sphaeroides* 2.4.1 where the energy of ^3C agrees with the in vitro energy, the energy of ^3C in RC of *R. rubrum* S1 is appreciably higher than its in vitro energy and must be influenced by the environment and/or the configuration of carotenoid in the RC.

The 2-fold higher ΔE of spheroidene in *Rb. sphaeroides* 2.4.1 compared to spirilloxanthine in *R. rubrum* would make the former carotenoid a much better quencher of ^3D. This is borne out by the $[^3C]/[^3D]$ ratio plotted in Fig. 6, which shows at approx. 150 K a 15-fold better quenching efficiency of spheroidene.

The EPR data of Frank et al. [62] suggest a large ΔE of ^3C in *Rb. sphaeroides* 2.4.1 compared to ^3C in the mutant *Rb. sphaeroides* G1C, which contains neurosporene. This agrees with the calculated in vitro ^3C energy of neurosporene, 0.90 eV (7280 cm^{-1}) (nine conjugated double bonds, [39]), giving an energy difference of -0.05 eV with the ^3D state of *Rb. sphaeroides* [63].

We note that the calculated [39] triplet energy of neurosporene is about 0.075 eV (600 cm^{-1}) higher than ^3D in *Rps. viridis* (which contains dihydroneurosporene [6]) [63]. This would effectively inhibit triplet transfer from D to C (see Discussion) but the considerable difference between in vitro and in vivo triplet energy found above for spirilloxanthin makes this explanation somewhat hazardous.

Mechanisms of triplet transfer

In the literature basically two mechanisms have been advanced to explain the temperature-dependence of D $\rightarrow$ C triplet transfer: (1) the reaction coordinate model, as proposed by Frank et al. [62] and (2) the intermediate state model, as proposed by Schenck et al. [38]. Our fit does not distinguish between these two models. In Fig. 5 we have depicted the two activation enthalpies in the reaction coordinate model, but it is obvious that an intermediate state model is equivalent when the lifetime of the intermediate is as short as suggested in Ref. 38 (10^{-12}–10^{-13} s).

In the reaction coordinate model the transfer of triplet excitation may be viewed to be analogous to an electron transport process. This is allowed since the current theories are homologous (see Ref. 15) for both phenomena. Thus, one may describe the transfer process as taking place along a reaction coordinate with two interacting potential curves (Fig. 6, inset). The two energies ΔE_a and ΔE follow naturally, without taking recourse to an intermediate triplet state. In this view, triplet transfer takes place either directly between D and C, or via superexchange mediated by B_B. The former possibility is not very probable, since direct triplet transfer necessitates orbital overlap (it is an exchange process) and the closest BChl of D, D_B, is about 10 Å away from carotenoid [16]. In model studies it has been found that the distance between carotenoid and the sensitizing pigment needs to be smaller than about 5 Å to promote efficient triplet transfer [64–66]. If superexchange plays a role, the obvious candidate for the bridging molecule is the accessory BChl of the B chain, B_B. This pigment would then mediate triplet transfer in a way analogous to the postulated function of B_A in electron transport [15].

The intermediate state of the model of Ref. 38 has not been identified. It was suggested that a $^3[D^+B^-]$ charge-transfer state was involved [38], but recent phosphorescence and EPR data make this unlikely [63,67]. Recently, it was proposed that B_B functions in this manner [68]. An attractive feature of this proposal is that ^3B_B of *Rps. viridis* has considerably higher energy than ^3B_B of *Rb. sphaeroides*, the energy difference with ^3D being about 200 (0.025 eV) and 1000 cm^{-1} (0.124 eV), respectively [68]. The former value is close to our value of $\Delta E = 160$ cm^{-1}. The above proposal explains in a natural way the observation that in *Rps. viridis* D $\rightarrow$ C triplet transfer does not occur [43,44]. There is at present, however, no evidence that an intermediate ^3B_B state exists; its short lifetime (about 10^{-12}–10^{-13} s according to Ref. 38) would make direct detection very difficult.

Another possible intermediate is the higher-energy exciton state of ^3D. The triplet state of a coupled dimer is formally described by the two Davydov components [69]:

$$^3D(+) = \alpha\, ^3D_A\, ^1D_B + \beta\, ^1D_A\, ^3D_B \quad (8a)$$

$$^3D(-) = \beta\, ^3D_A\, ^1D_B - \alpha\, ^1D_A\, ^3D_B \quad (8b)$$

in which $\alpha^2 + \beta^2 = 1$ and the $(-)$ combination has the higher energy. α and β depend on the extent of localization, which in turn depends on the energy difference between the unperturbed ^3D_A and ^3D_B states (so-called site-splitting induced by deviations from C_2 symmetry) and the exchange interaction J between D_A and D_B. For a fully delocalized, symmetric ^3D state $\alpha = \beta = \frac{1}{2}\sqrt{2}$. For a completely localized ^3D state either α or β equals zero. In Eqn. 8 charge-transfer contributions are neglected.

Exciton calculations [31,45,70] and EPR measurements [71] have found the triplet state on D to be (partly) localized at temperatures below 10 K. For RC of *Rps. viridis* at 1.2 K a 75–100% localization on D_A was found [31,70,71], while for RC of *Rb. sphaeroides* R-26 and *Chloroflexus aurantiacus* at 1.2 K the triplet

state appears to be localized on the B side of the BChl dimer for 70 and 95%, respectively [45].

If C couples (possibly via superexchange) to ^3D_B but not to ^3D_A and if $\alpha \gg \beta$, then the lower energy $^3D(+)$ state would couple little to C and at low temperatures triplet transfer to C would be inhibited. At higher temperatures, however, the $^3D(-)$ state would become populated and triplet transfer would be promoted via the second term in the right-hand side of Eqn. 8b. Thus, in this view, the activation enthalpy is needed to change the site of localization of the triplet state. Neglecting volume changes, the exicton splitting would then be about 160 cm^{-1}. This value is much larger than values normally found for the exchange energy in molecular crystals and would thus be largely due to site-splitting, in keeping with the idea of a localized triplet state ($\alpha \gg \beta$).

In principle, temperature-induced changes in the distance between C and D could also explain the temperature-dependence of the ^3C yield. In that case, however, this change must also affect the high efficiency of the S–S $^1C^*$-$^1D^*$ transfer, since this process is probably likewise governed by exchange interaction (Dexter transfer) [6]. This has been checked by Schenck et al. [38] by measuring the action spectrum of this process as function of the temperature. No clear temperature-induced changes were observed in the S–S transfer efficiency.

If the model of triplet transfer described above is correct, then one would expect the following. (a) In *Rb. sphaeroides* 2.4.1 and in *R. rubrum* S1 the triplet state is predominantly localized at low temperatures. The site of localization depends on whether carotenoid couples more strongly to D_A or to D_B. Since coupling presumably proceeds via B_B, which is closer to D_A than to D_B [3], ^3D would then be localized on D_B. (b) In *Rps. viridis* the site-splitting (and hence the local asymmetry of D) is much larger than in the BChl *a*-containing species. Both predictions can be tested experimentally: (a) by performing LD-ADMR and EPR experiments as in Refs. 31 and 71, (b) by high-resolution X-ray crystallography. We note that in *Rb. sphaeroides* R-26 and in *Chl. aurantiacus* due to the absence of a carotenoid and the replacement of B_B by a BPh molecule, respectively, the local symmetry (and hence the sidedness of the triplet localization) need not be the same as in the species studied here.

Conclusions

1. From the temperature-dependence of (T – S) spectra between 10 and 288 K the ^3C yield has been determined as a function of the temperature. The mechanism of triplet transfer between D and C is discussed for reaction centers of *Rb. sphaeroides* 2.4.1 and *R. rubrum* S1.
2. With a kinetic equilibrium model the activation enthalpies of triplet transfer $^3D \rightarrow C$ and $^3C \rightarrow D$ have been determined (0.020 and 0.15 eV for *Rb. sphaeroides* 2.4.1, respectively, and 0.020 and 0.08 eV for *R. rubrum* S1, respectively). If volume changes are neglected, this yields for the energy difference between the ^3D and ^3C states 0.13 eV for *Rb. sphaeroides* 2.4.1 and 0.06 eV for *R. rubrum* S1.
3. Triplet transfer between D and C can be mediated by higher vibrational states of ^3D and ^3C (the reaction coordinate model) or by an intermediate, for which the accessory B_B molecue or the higher-energy triplet exciton state of ^3D are candidates. In the latter case, the exciton splitting of the ^3D is large and is mainly due to environmental effects (site-splitting).
4. From the fact that the BChl peak at 807 nm is maximally bleached at the same temperature at which the ^3C yield is maximal, we conclude that the carotenoid shares its triplet exciton with the neighboring accessory BChl. This conclusion may be tested by reconstituting borohydride-treated RC of *Rb. spaeroides* R-26 with carotenoid.

Acknowledgements

Ms. H.M. Nan and M. Maas prepared the reaction centers. We thank Mr. C.A. Bauer for assisting with some of the experiments. We are indebted to Dr. J. Schmidt and his colleagues of the Center for the Study of Excited States of Molecules for their hospitality and for making some of their laboratory space and equipment available to us. This work was supported by the Netherlands Foundation for Chemical Research (SON), financed by the Netherlands Organization for Scientific Research (NWO).

References

1 Deisenhofer, J., Epp. O., Miki, K., Huber, R. and Michel, H. (1984) J. Mol. Biol. 180, 385–398.
2 Chang, C.-H., Tiede, D., Tang, J., Smith, U., Norris, J. and Schiffer, M. (1986) FEBS Lett. 205, 82–86.
3 Allen, J.P., Feher, G., Yeates, T.O., Komiya, H. and Rees, D.C. (1987) Proc. Natl. Acad. Sci. USA 84, 5730–5734; 6162–6166.
4 Martin, J.-L., Breton, J., Hoff, A.J., Migus, A. and Antonetti, A. (1986) Proc. Natl. Acad. Sci. USA 83, 957–961.
5 Schenck, C.C., Blankenship, R.E. and Parson, W.W. (1982) Biochim. Biophys. Acta 680, 44–59.
6 Cogdell, R.J. and Frank, H.A. (1988) Biochim. Biophys. Acta 895, 63–79.
7 Lutz, M., Szponarski, W., Berger, G., Robert, B. and Neumann, J.M. (1987) Biochim. Biophys. Acta 894, 423–433.
8 Lutz, M., Robert, B., Zhou, Q., Neumann, J.M., Szponarski, W. and Berger, G. (1988) in The Photosynthetic Bacterial Reaction Center, Structure and Dynamics (Breton, J. and Vermeglio, A., eds.), pp. 41–50, Plenum Press, New York.
9 Koyama, Y., Kanaji, M. and Shimamura, T. (1988) Photochem. Photobiol. 48, 107–114.
10 Boucher, F., Van der Rest, M. and Gingras, G. (1977) Biochim. Biophys. Acta 461, 339–357.

11 Dallinger, R.F., Farquharson, S., Woodruff, W.H. and Rodgers, M.A.J. (1981) J. Am. Chem. Soc. 103, 7433–7440.
12 Schmidt, K. (1978) in The Photosynthetic Bacteria (Clayton, R.K. and Sistrom, W.R., eds.), pp. 729–750, Plenum Press, New York.
13 Chadwick, B.W. and Frank, H.A. (1986) Biochim. Biophys. Acta 851, 257–266.
14 Scheer, H., Beese, D., Steiner, R. and Angerhofer, A. (1988) in The Photosynthetic Bacterial Reaction Center, Structure and Dynamics (Breton, J. and Vermeglio, A., eds.), pp. 101–111, Plenum Press, New York.
15 Michel-Beyerle, M.E., Plato, M., Deisenhofer, J., Michel, H., Bixon, M. and Jortner, J. (1988) Biochim. Biophys. Acta 932, 52–70.
16 Allen, J.P., Feher, G., Yeates, T.O., Komiya, H. and Rees, D.C. (1988) in The Photosynthetic Bacterial Reaction Center, Structure and Dynamics (Breton, J. and Vermeglio, A., eds.), pp. 5–11, Plenum Press, New York.
17 Hoff, A.J., Lous, E.J., Möhl, K.W. and Dijkman, J.A. (1985) Chem. Phys. Lett. 114, 39–43.
18 Lous, E.J. and Hoff, A.J. (1986) Photosynth. Res. 9, 89–101.
19 Lous, E.J. and Hoff, A.J. (1988) in The Photosynthetic Bacterial Reaction Center, Structure and Dynamics, (Breton, J. and Vermeglio, A. eds.), pp. 71–88, Plenum Press, New York.
20 Hoff, A.J. (1981) Quart. Rev. Biophys. 14, 559–665.
21 Blankenship, R.E., Schaafsma, T.J. and Parson, W.W. (1977) Biochim. Biophys. Acta 461, 297–305.
22 Hoff, A.J., Rademaker, H., Van Grondelle, R. and Duysens, L.N.M. (1977) Biochim. Biophys. Acta 460, 547–554.
23 Lersch, W. and Michel-Beyerle, M.E. (1983) Chem. Physics 78, 115–126.
24 Budil, D.E., Kolaczkowski, S.V. and Norris, J.R. (1987) in Progress in Photosynthesis Research (Biggins, J., ed.), pp. 25–28, Martinus Nijhoff, Dordrecht.
25 Wertz, J.E. and Bolton, J.R. (1972) Electron Spin Resonance: Elementary Theory and Practical Applications, McGraw-Hill, New York.
26 Clarke, R.H., Connors, R.E. and Keegan, J. (1977) J. Chem. Phys. 66, 358–359.
27 De Vries, H.G. and Hoff, A.J. (1978) Chem. Phys. Lett. 55, 395–398.
28 Lous, E.J. (1988) Doctoral dissertation, Leiden.
29 Den Blanken, H.J., Meiburg, R.F. and Hoff, A.J. (1984) Chem. Phys. Lett. 105, 336–342.
30 Hoff, A.J., Den Blanken, H.J., Vasmel, H. and Meiburg, R.F. (1985) Biochim. Biophys. Acta 806, 389–397.
31 Lous, E.J. and Hoff, A.J. (1987) Proc. Natl. Acad. Sci. USA 84, 6147–6151.
32 Cohen-Bazire, G., Sistrom, W.R. and Stanier, R.Y. (1957) J. Cell Comp. Physiol. 49, 25–68.
33 Vadeboncoeur, C., Mamet-Bratley, M. and Gingras, G. (1979) Biochemistry 18, 4308–4314.
34 Noel, H., Van der Rest, M. and Gingras, G. (1972) Biochim. Biophys. Acta 275, 219–230.
35 Smith, W.R., Sybesma, C. and Dus, K. (1972) Biochim. Biophys. Acta 267, 609–615.
36 Wang, R.T. and Clayton, R.K. (1973) Photochem. Photobiol. 17, 57–61.
37 Cogdell, R.J., Monger, T.G. and Parson, W.W. (1975) Biochim. Biophys. Acta 408, 189–199.
38 Schenck, C.C., Mathis, P. and Lutz, M. (1984) Photochem. Photobiol. 39, 407–417.
39 Bensasson, R., Land, E.J. and Maudinas, B. (1976) Photochem. Photobiol. 23, 118–193.
40 Douzou, P. and Petsko, G.A. (1984) Adv. Protein Chem. 36, 245–361.
41 Rafferty, C.N. and Clayton, R.K. (1979) Biochim. Biophys. Acta 545, 106–121.
42 Knapp, E.W., Fischer, S.F., Zinth, W., Sander, M., Kaiser, W., Deisenhofer, J. and Michel, H. (1985) Proc. Natl. Acad. Sci. USA 82, 8463–8467.
43 Holten, D., Windsor, M.W., Parson, W.W. and Thornber, J.P. (1978) Biochim. Biophys. Acta 501, 112–126.
44 Lous, E.J. and Hoff, A.J. (1987) in Progress in Photosynthesis Research (Biggins, J., ed.) pp. 197–200, Martinus Nijhoff, Dordrecht.
45 Scherer, P.O.J. and Fischer, S.F. (1987) Biochim. Biophys. Acta 891, 157–164.
46 Kirmaier, C., Holten, D. and Parson, W.W. (1985) Biochim. Biophys. Acta 810, 49–61.
47 Kirmaier, C. and Holten, D. (1988) In The Photosynthetic Bacterial Reaction Center, Structure and Dynamics (Breton, J. and Vermeglio, A., eds.), pp. 219–228, Plenum Press, New York.
48 Hoganson, C.W., Windsor, M.W., Farkas, D.I. and Parson, W.W. (1987) Biochim. Biophys. Acta 892, 275–283.
49 Clayton, R.K. and Devault, D. (1972) Photochem. Photobiol. 15, 165–175.
50 Jortner, J. (1976) J. Chem. Phys. 64, 4860–4867.
51 Hoff, A.J. (1982) in Light Reaction Path of Photosynthesis (F.K. Fong, ed.), pp. 80–151, Springer-Verlag, New York.
52 Martin, J.-L., Breton, J., Lambry, J.C. and Fleming, G.R. (1988) in The Photosynthetic Bacterial Reaction Center, Structure and Dynamics (Breton, J. and Vermeglio, A., eds.), pp. 195–203, Plenum Press, New York.
53 Meech, S.R., Hoff, A.J. and Wiersma, D.A. (1986) Proc. Natl. Acad. Sci. USA 83, 9464–9468.
54 Boxer, S.G., Lockhart, D.J. and Middendorf, T.R. (1986) Chem. Phys. Lett. 123, 476–482.
55 Scherer, P.O.J., Fischer, S.F., Hörber, J.K.H., Michel-Beyerle, M.E. and Michel, H. (1985) in Antennas and Reaction Centers of Photosynthetic Bacteria (Michel-Beyerle, M.E., ed.), pp. 131–137, Springer-Verlag, Berlin.
56 Hayes, J.M., Gillie, J.K., Tang, D. and Small, G.J. (1988) Biochim. Biophys. Acta 932, 287–305.
57 Straley, S.C., Parson, W.W., Mauzerall, D.C. and Clayton, R.K. (1973) Biochim. Biophys. Acta 305, 597–609.
58 Loach, P.A. and Walsh, K. (1969) Biochemistry 8, 1908–1913.
59 Clayton, R.K. and Yamamoto, T. (1976) Photochem. Photobiol. 24, 67–70.
60 Scherer, P.O.J. and Fisher, S.F. (1986) Chem. Phys. Lett. 131, 153–159.
61 Chidsey, C.E.D., Takiff, L., Goldstein, R.A. and Boxer, S.G. (1985) Proc. Natl. Acad. Sci. USA 82, 6850–6854.
62 Frank, H.A., Machnicki, J. and Friesner, R. (1983) Photochem. Photobiol. 38, 451–455.
63 Takiff, L. and Boxer, S.G. (1988) Biochim. Biophys. Acta 932, 325–334.
64 Liddell, P.A., Nemeth, G.A., Lehman, W.R., Joy, A.M., Moore, A.L., Bensasson, R.V., Moore, T.A. and Gust, D. (1982) Photochem. Photobiol. 36, 641–645.
65 Gust, D., Moore, T.A., Bensasson, R.V., Mathis, P., Land, E.J., Chachaty, C., Moore, A.L., Liddell, P.A. and Nemeth, G.A. (1985) J. Am. Chem. Soc. 107, 3631–3640.
66 Wasielewski, M.R., Liddell, P.A., Barrett, D., Moore, T.A. and Gust, D. (1986) Nature 322, 570–572.
67 Hoff, A.J. and Proskuryakov, I.I. (1985) Chem. Phys. Lett. 115, 303–310.
68 Takiff, L. and Boxer, S.G. (1988) J. Am. Chem. Soc. 110, 4425–4426.
69 Davydov, A.S. (1971) Theory of Molecular Excitons, Plenum Press, New York.
70 Knapp, E.W., Scherer, P.O.J. and Fischer, S.F. (1986) Biochim. Biophys. Acta 852, 295–305.
71 Norris, J.R., Lin, C.P. and Budil, D.E. (1987) J. Chem. Soc. Faraday Trans. 1, 83, 13–27.
72 Slooten, L. (1973) Doctoral dissertation, Leiden.